A Structural Investigation of Hydrous and Anhydrous Rare-Earth Phosphates

Mohamed Ruwaid Rafiuddin and Andrew P. Grosvenor*

Department of Chemistry, University of Saskatchewan, Saskatoon, SK, Canada, S7N 5C9

* Author to whom correspondence should be addressed

E-mail: andrew.grosvenor@usask.ca

Phone: (306) 966-4660

Fax: (306) 966-4730

Abstract

Rhabdophane- ($REPO_4.nH_2O$; RE = La to Dy), Monazite- ($REPO_4$; RE = La to Gd), Xenotime- ($REPO_4$ & $RE'PO_4.nH_2O$; RE = Tb to Lu and Y; RE' = Ho to Lu and Y) type rare-earth phosphate materials are being considered for a number of applications including as photonic materials, for biolabeling studies, and as potential nuclear wasteforms. Structural studies of hydrous rare-earth phosphates are rather limited when compared to anhydrous rare-earth phosphates. In this study, rhabdophane- ($REPO_4.nH_2O$; RE = La, Nd, Sm, Gd, and Dy) and xenotime- ($REPO_4.nH_2O$; RE = Y and Yb) type materials were synthesized by a precipitation-based method and investigated using X-ray diffraction (XRD) and X-ray absorption near-edge spectroscopy (XANES). Examination of the powder XRD data from rhabdophane-type materials has confirmed that the rhabdophane structure crystallizes in the monoclinic crystal system rather than the hexagonal structure that has most often been reported. Materials adopting the rhabdophane- or xenotime- type structure were studied as a function of temperature to understand how the structure varies with increasing annealing temperature. Local structural information was obtained by collecting P K- and RE L_1- edge XANES spectra. Examination of P K-edge XANES spectra from rhabdophane- and xenotime- type materials revealed changes in the local environment around P as a function of temperature. These changes were attributed to the removal of water from these structures as a result of high temperature annealing.

1. Introduction

Rare-earth phosphates are an interesting class of materials that have applications as nuclear wasteforms, in photonics, as proton conductors, as catalysts, and in biolabeling.[1–8] These applications stem from the structural diversity exhibited by these compounds. Depending on the size of the rare-earth ions and the synthetic methods used, the rare-earth phosphates can adopt the rhabdophane- ($REPO_4.nH_2O$; RE = La to Dy), monazite- ($REPO_4$; RE = La to Gd), or xenotime- ($REPO_4$ & $RE'PO_4.nH_2O$; RE = Tb to Lu and Y; RE' = Ho to Lu and Y) type structure.[9–13]

Anhydrous rare-earth phosphates adopting the monazite- and xenotime-type structures have been widely studied due to their potential use as a crystalline matrix for the immobilization of actinides.[1,14,15] Rhabdophane, on the other hand, is formed during the aqueous alteration of rare-earth minerals (e.g., monazite) and could play a role in controlling the solubility of actinides.[12,16] It has been reported that the rhabdophane phase forms on the surface of leached monazite pellets and may act as a protective barrier by either delaying or stopping the release of actinides to the environment.[12,16] In contrast to the monazite and xenotime structures, structural studies of the rhabdophane-type materials are rather limited due to their metastable nature.[17] The rhabdophane structure initially loses water upon heating to form an anhydrous compound followed by an irreversible structural transformation to the monazite- or xenotime- type structure depending on the rare-earth present when annealed at higher temperatures.[17] Materials adopting the rhabdophane-type structure are usually synthesized in powder form by solution based synthetic methods and no instances of single crystal growth of these materials have been reported in the literature.[18,19] The authors of the current study are aware of only two studies in which the

crystal structure of rhabdophane ($REPO_4.nH_2O$) was determined using powder X-ray diffraction (XRD).[11,12]

Evidence for the existence of the rhabdophane-type structure was first reported by Mooney.[10,11] Mooney found that the phosphates of La, Ce, and Nd crystallized in two forms: monoclinic (monazite) or hexagonal ($REPO_4.nH_2O$) crystal systems.[10,11] The hexagonal structure (Space group – $P6_222$ or $P3_121$) of the hydrated rare-earth phosphates was proposed based on the analysis of diffraction photographs taken from powder samples.[11] Recently, Mesbah et al. reported that the use of a hexagonal model for the Rietveld refinement of synchrotron powder XRD data collected from polycrystalline rhabdophane ($SmPO_4.0.667H_2O$) led to a poor refinement.[12] The crystal structure of rhabdophane ($SmPO_4.0.667H_2O$) was solved ab-initio by Mesbah et al., with the results indicating that rhabdophane-type materials adopt a monoclinic (Space group – $C2$) structure.[12] It should be noted that a large body of work is available on the luminescent properties of rhabdophanes in which the crystal structure is considered to be hexagonal.[20–24]

The crystal structure of monoclinic rhabdophane (e.g., $SmPO_4.H_2O$) is shown in Figure 1a.[12] The structure comprises of two chains referred to as Ch1 and Ch2 (See Figure 1b). There is an alternating sequence of Sm-O polyhedra and PO_4 tetrahedra along the 'a' direction in both chains (Figure 1b).[12] The alternating PO_4 tetrahedra in Ch1 have four different P-O bond distances and P-O-P bond angles whereas in Ch2, the level of distortion in the alternating PO_4 tetrahedra is not uniform (i.e., four distinct P-O bond distances and P-O-P bond angles in the first tetrahedra followed by two distinct P-O bond distances and P-O-P bond angles in the second tetrahedra). The Sm ions in chains Ch1 and Ch2 differ in terms of their coordination environment. The Sm ions in Ch1 are bonded to nine oxygen atoms (eight provided by the PO_4

groups and one from water) and in Ch2, the Sm atoms are coordinated to only eight oxygen atoms provided by the PO_4 groups (Figure 1b).[12] Both SmO_9 and SmO_8 polyhedra are distorted. The connection of the two chains leads to the formation of infinite channels running along the 'a' direction. Each channel is formed by the connection of six chains (4 Ch1 and 2 Ch2) and water resides inside these channels (Figure 1a).[12] For more detailed information on the structure of monoclinic rhabdophane, the reader is referred to the article by Mesbah et al.[12] Materials adopting the rhabdophane structure undergo a structural change to the more stable monazite- or xenotime- type structures upon heating to higher temperatures.[17] The crystal structures of monazite (e.g., $CePO_4$; space group – $P2_1/n$) and xenotime (e.g., YPO_4; space group – $I4_1/amd$) are presented in Figures 1c and 1d.[13] The Ce^{3+} ions in the monazite structure are coordinated to nine O atoms and the resulting CeO_9 polyhedra are connected to each other via distorted PO_4 tetrahedra (Figure 1c).[13] In the xenotime structure, the Y^{3+} ions are surrounded by eight O atoms and the resulting YO_8 polyhedra are connected to each other via symmetric PO_4 tetrahedra (Figure 1d).[13] More information about the crystal structures of monazite- and xenotime- type rare-earth phosphates can be found elsewhere.[13,26]

A structural investigation of the hydrous and anhydrous type rare-earth phosphates was carried out in this study using powder XRD and X-ray absorption near-edge spectroscopy (XANES). XANES spectra are element specific and offer information on the local electronic structure around the absorbing atom.[27] The $REPO_4.nH_2O$ (RE = La, Nd, Sm, Gd, Dy, Y, Yb) and $Gd_{1-x}Dy_xPO_4.nH_2O$ (x = 0.0, 0.2, 0.4, 0.8, 1.0) materials were synthesized using a precipitation route with the crystal structure adopted by the as-synthesized materials being observed to depend on the size of the RE ion.[18] The as-synthesized materials were annealed at various temperatures and studied by powder XRD in order to examine changes in the long-range structure of these

materials. Information about the local structure of the RE and P ions in the as-synthesized and annealed materials was obtained from the analysis of RE L_1- (RE = Gd, Dy, Sm), RE L_3-, P K-, and P $L_{2,3}$- edge XANES spectra. To the best of our knowledge, this represents the first study to investigate variations in the local structure of $REPO_4.nH_2O$ (RE = La, Nd, Sm, Gd, Dy, Y, Yb) materials with varying annealing temperature. The primary objective of this study was to understand how the long-range and local structure of $REPO_4.nH_2O$ materials changed as a function of temperature and size of the RE ion.

2. Experimental section

2.1. Synthesis and powder XRD

The hydrated rare-earth phosphates ($REPO_4.nH_2O$ and $Gd_{1-x}Dy_xPO_4.nH_2O$ [x = 0.0, 0.2, 0.4, 0.8, 1.0]; RE = La, Nd, Sm, Gd, Dy, Y, Yb) were synthesized following the procedure developed by Kijkowska.[18] La_2O_3 (Alfa Aesar; 99.99%), Nd_2O_3 (Alfa Aesar; 99.9%), Sm_2O_3 (Alfa Aesar; 99.9%), Gd_2O_3 (Alfa Aesar; 99.99%), Dy_2O_3 (Alfa Aesar; 99.9%), Y_2O_3 (Alfa Aesar; 99.99%), Yb_2O_3 (Alfa Aesar; 99.9%), and H_3PO_4 (Fisher Scientific; 85%) were used as the starting materials. Finely ground powders of RE_2O_3 (0.0020 moles) were added to a beaker containing 13.7 mL of 14.6 M H_3PO_4 (0.200 moles) and the resulting mixture was stirred until a clear solution was obtained. A PO_4:RE_2O_3 mole ratio of 100:1 was used to synthesize these compounds. It must be noted here that the mixture containing Nd_2O_3 and H_3PO_4 remained cloudy even after stirring for long periods of time (~1 day); however, a clear solution was obtained while using other RE_2O_3 (RE = La, Sm, Gd, Dy, Y, and Yb) oxides. The clear or cloudy solution was then diluted through the addition of 100 mL of water. This solution was then transferred to a round bottomed flask and refluxed at ~130°C for 2 hours. The clear solution

containing La ions became cloudy immediately after the addition of 100 mL of water while the solutions containing other RE ions (RE = Sm, Gd, Dy, Y, Yb) remained clear. The resulting precipitate was filtered and washed using deionized water after refluxing and then dried in air overnight before being heated at 60°C for 1 hour.

The phase purity and the crystal structure of the as-synthesized materials ($REPO_4.nH_2O$ [RE = La, Nd, Sm, Gd, Dy, Y, Yb] and $Gd_{1-x}Dy_xPO_4.nH_2O$ [x = 0.0, 0.2, 0.4, 0.8, 1.0]) was determined by analysis of powder XRD patterns collected using a PANalytical Empyrean system (Co $K\alpha_{1,2}$ or Cu $K\alpha_{1,2}$ X-ray source). Powder XRD patterns were also collected from $REPO_4.nH_2O$ (RE = La, Nd, Sm, Gd, Dy, Y, Yb) materials annealed at different temperatures (500°C -1200°C) for 12h (followed by quench cooling in air) in order to study the effect of annealing temperature on the long-range order of these materials. Powder XRD patterns from the as-synthesized and annealed materials were collected in the 2θ range of 10°-80° using a step size of 0.017° and the lattice constants were determined using the HighScore Plus software program.[28] The powder XRD pattern from as-synthesized $DyPO_4.nH_2O$ (rhabdophane-type structure) was refined using the hexagonal and the monoclinic structural models to determine the best structure to describe this phase.[11,12] For refinement purposes, the powder XRD pattern from $DyPO_4.H_2O$ was collected over a wide 2θ range (5° - 120°) using a step size of 0.017° with the data being refined over the 2θ range of 10°-80°. The following parameters were varied during the refinement: scale factors, zero shift, lattice constants, profile variables, and the overall isotropic thermal factor (B_{OVL}). The atomic positions were fixed during the refinement.

2.2. Thermogravimetric analysis (TGA)

Thermogravimetric analysis was performed using a TA Instrument Q5000 TGA instrument to determine the total water content in the as-synthesized materials. Powdered samples of $DyPO_4.nH_2O$ (rhabdophane-type) and $YbPO_4.nH_2O$ (xenotime-type) weighing ~17 mg were heated in air (25.0 ml/min) in a Pt pan from 25°C to 700°C at 5°C/min with the weight loss being constantly monitored.

2.3. XANES

2.3.1. P K-edge XANES

The P K-edge XANES spectra from the as-synthesized and annealed $REPO_4.nH_2O$ (RE = Sm, Gd, Dy, Yb) materials were collected using the Soft X-ray Micro-characterization Beamline (SXRMB; 06B1-1) located at the Canadian Light Source (CLS).[29] A Si (111) double crystal monochromator was used and the spectral resolution was 0.2 eV at 2145.5 eV (P K-edge).[29] Fine powders of $REPO_4.nH_2O$ were mounted on carbon tape and the spectra were measured in vacuum in partial fluorescent yield (PFY) mode with a step size of 0.15 eV through the absorption edge. Calibration of P K-edge spectra was performed by collecting a spectrum from red P with the maximum in the first derivative being set to 2145.5 eV.[30] All spectra discussed in this study were analyzed using the Athena software program.[31]

2.3.2. P $L_{2,3}$-edge XANES

The P $L_{2,3}$-edge XANES spectra were collected from as-synthesized and annealed $DyPO_4.nH_2O$ materials using the Variable Line Spacing-Plane Grating Monochromator (VLS-PGM; 11ID-2) beamline at the CLS.[32] A high energy grating monochromator was used to collect

the P $L_{2,3}$-edge spectra and the spectral resolution was 0.01 eV at 130 eV (P L_3-edge). The samples were finely ground before placing them on carbon tape and the spectra were measured in vacuum in total fluorescent yield (TFY) mode using a step size of 0.05 eV through the absorption edge. The P $L_{2,3}$-edge spectra were calibrated by collecting a spectrum from red P and setting the maximum in the first derivative to 130 eV.

2.3.3. RE L_1- and L_3-edge (RE = Sm, Gd, Dy) XANES

The RE L_1- and L_3- edge XANES spectra from $REPO_4.nH_2O$ (RE = Sm, Gd, Dy, Yb) were collected using the Sector 20 – Bending Magnet (20 BM; CLS@APS) beamline located at the Advanced Photon Source (APS; Argonne National Laboratory).[33] The spectra were collected in transmission mode using a Si (111) double crystal monochromator and 100% N_2 gas filled ionization chambers. The spectral resolution varied from 0.9 eV at 6716 eV (Sm L_3-edge) to 1.5 eV at 10486 eV (Yb L_1-edge). Fine powders of the materials were sandwiched between layers of kapton tape and the absorption signal was maximized by adjusting the number of layers. The XANES spectra were collected using a step size of 0.15 eV through the RE L_1- and RE L_3-edges. Spectra from the calibration standards were collected from metal foils placed between the transmission and reference ionization chambers. The Gd L_3-, Dy L_3-, and Sm L_1- edge spectra were calibrated using Co metal foil (E_0 = 7709 eV). The Gd L_1-, Dy L_1-, Sm L_3-, Yb L_1- edge spectra were calibrated using Ni (E_0 = 8333 eV), Zn (E_0 = 9659 eV), Fe (E_0 = 7112 eV), and Ga (E_0 = 10367) metal foils, respectively.[30]

3. Results and Discussion

3.1. TGA and Powder XRD

The as-synthesized $REPO_4.nH_2O$ materials were found by XRD (*vide infra*) to adopt one of two structure types: rhabdophane (RE = La, Nd, Sm, Gd, Dy) or xenotime (RE = Y, Yb).[12,13] The water content 'n' in the rhabdophane and xenotime structures was determined by performing TGA on $DyPO_4.nH_2O$ and $YbPO_4.nH_2O$ (Figure S1 in the supporting information). In accordance with previous studies, two distinct regions were observed in the TGA plot from rhabdophane and are attributed to the two-step elimination of water (Figure S1a in the supporting information).[9] However, in materials adopting the xenotime-type structure, a continuous weight loss was observed in the temperature range of 25ºC-700°C (Figure S1b in the supporting information).[9] The value of 'n' was determined to be ~1 for both structures and represents the total water content (i.e., no distinction was made between adsorbed and lattice water in this study). This result is in agreement with a previous investigation of these materials.[9] The total water content in the rhabdophane- and xenotime- type structures appears to be removed once the temperature reaches ~700°C.

Two different crystal structures (hexagonal and monoclinic) are reported for compounds adopting the rhabdophane structure.[11,12] The crystal structure of the rhabdophane-type materials was determined by performing a Rietveld refinement of the powder XRD data from $DyPO_4.H_2O$ using the hexagonal and monoclinic structural models (Figure 2).[11,12] Large differences in peak intensity were observed between the calculated and observed patterns when the hexagonal model was used (Figure 2a). In contrast, a significantly better fit was obtained using the monoclinic model as indicated by the residual pattern in Figure 2b. The lattice constants and fit parameters

for $DyPO_4.H_2O$ obtained using the hexagonal and monoclinic structural models are listed in Table 1. It is concluded here that the rhabdophane materials studied adopt the monoclinic structure.[12]

The powder XRD patterns from materials adopting the rhabdophane ($REPO_4.H_2O$; RE = La, Nd, Sm, Gd, Dy) structure are presented in Figure 3a. Significant variations in peak widths and intensity were observed across the rhabdophane series. The presence of broad diffraction peaks in the XRD patterns from $LaPO_4.H_2O$ and $NdPO_4.H_2O$ indicate that these materials are poorly crystalline. On moving from $LaPO_4.H_2O$ to $DyPO_4.H_2O$, the peaks became narrower and more intense, indicating an increase in the crystallinity of these materials. This observation agrees well with an earlier report wherein similar observations were made through the analysis of scanning electron micrographs.[18] The lattice constants of the materials adopting the rhabdophane structure are listed in Table 2. In addition to the ternary compounds, a $Gd_{1-x}Dy_xPO_4.H_2O$ (x = 0.0, 0.2, 0.4, 0.8, 1.0) solid solution was also synthesized. The XRD patterns confirmed that all members of the solid solution adopt the rhabdophane structure (Figure 3b). The diffraction peaks shifted to higher 2θ with increasing Dy substitution thereby indicating a contraction in the unit cell, which is in agreement with the lower ionic radius of Dy^{3+} compared to Gd^{3+} (Figure 3b and Table S1 in the supporting information).[34]

The water content in the rhabdophane structure was determined to be eliminated at ~700°C by TGA (*vide supra*) and it was of interest to study how the long-range structure of rhabdophane-type materials changed upon removal of water. The long-range structure of rhabdophane was studied as a function of temperature by examining the powder XRD patterns from $DyPO_4.H_2O$ samples annealed at different temperatures (600°C-1100°C) (Figure 4). In comparison to the as-synthesized material, substantial changes in the powder XRD patterns from

the materials annealed at 600°C and 700°C were not observed (Figure 4a). These results suggest that the long-range structure of rhabdophane is not significantly affected by the absence of water. At higher annealing temperatures (> 700°C), the structure of $DyPO_4$ initially transformed to a mixture of monazite- and xenotime- type structures before undergoing a final transformation to the xenotime structure at temperatures exceeding 800°C (Figure 4b). The temperature at which the rhabdophane → monazite and/or xenotime transformation occurs was different for the compounds in the rhabdophane series ($500°<T\leq700°C$), and was observed to increase with a decrease in the size of the rare-earth (RE = La, Sm, Gd, Dy) ions (See Figure 4b and Figure S2 in the supporting information).

It has been reported that the structural transformation of $REPO_4.H_2O$ (rhabdophane-type) to $REPO_4$ (monazite- or/and xenotime-type) at high-temperature is accompanied by the formation of minor amounts of rare-earth polytrioxophosphate (REP_3O_9).[35,36] The as-synthesized precipitate may contain adsorbed H_3PO_4 that can react with $REPO_4.H_2O$ at higher temperatures to form REP_3O_9.[35,36] However, in the present study, the REP_3O_9 (RE = La, Nd, Sm, Gd, Dy) phase was not observed during the structural transformation of rhabdophane- to monazite- and/or xenotime-type structures. This is because the as-synthesized precipitates of $REPO_4.H_2O$ were washed with a large excess of water prior to annealing to remove any adsorbed phosphates.

The as-synthesized $YbPO_4.H_2O$ (and $YPO_4.H_2O$) materials were determined by analysis of powder XRD patterns to adopt the xenotime-type structure (Figure 5).[13] The xenotime-type structure crystallizes in a tetragonal unit cell which is of higher symmetry when compared to the monoclinic unit cell adopted by the rhabdophane structure.[12,13] The long-range structure of $YbPO_4.H_2O$ was studied as a function of temperature by collecting powder XRD patterns from $YbPO_4.H_2O$ annealed to 600°C and 1200°C (Figure 5). Upon heating to 600°C, the diffraction

peaks become broader and shifted slightly to higher 2θ (See inset in Figure 5). These observations suggest a decrease in crystallinity as well as a contraction in the unit cell of the xenotime-type structure upon removal of water. Further heating to 1200°C results in an improvement in the crystallinity of the material as indicated by the presence of intense and narrow diffraction peaks (Figure 5). In contrast to the rhabdophane structure, the xenotime-type structure was stable at all annealing temperatures as indicated by the powder XRD patterns from $YbPO_4.H_2O$ annealed at 600°C or 1200°C (Figure 5). The lattice constants of as-synthesized $YbPO_4.H_2O$ are presented in Table 3 along with the lattice constants from this material after annealing at 600°C or 1200°C. A slightly larger unit cell was observed for the as-synthesized material in comparison to the materials annealed to 600°C or 1200°C. These observations are consistent with an earlier report in which a similar contraction in the unit cell parameters of xenotime-type materials was observed after annealing $ErPO_4.H_2O$ (also prepared using a precipitation route) to 950°C.[9] These results indicate that the presence of water introduces changes in the xenotime crystal structure; however, more detailed studies on $YbPO_4.H_2O$ are required in order to explain how water affects the local and long-range structure.

3.2. XANES

The effect of annealing temperature on the long-range order of materials adopting the rhabdophane- and xenotime- type structures was discussed in Section 3.1 through the analysis of powder XRD data. It was shown that the powder XRD data of $DyPO_4.H_2O$ (rhabdophane-type) annealed to 700°C did not exhibit significant changes in the long-range order of the rhabdophane-type structure upon removal of water whereas distinct (although minor) changes in the powder XRD pattern of $YbPO_4.H_2O$ were observed with increasing annealing temperature. XANES spectra were collected from the $REPO_4.H_2O$ (RE = Sm, Gd, Dy, Yb) materials in order

to determine how the local structures of these materials are affected by the loss of water. Temperature-induced changes in the local coordination environment of P and RE (RE = Sm, Gd, Dy, Yb) ions were probed by examination of P K-, P $L_{2,3}$-, and RE L_1- edge XANES spectra.

3.2.1. P K-edge XANES

The P K-edge XANES spectra from as-synthesized $Gd_{1-x}Dy_xPO_4.H_2O$ (x = 0, 0.2, 0.4, 0.8, 1; rhabdophane-type structure) are presented in Figure 6 and represent the dipole allowed excitation of P 1s electrons into unoccupied P 3p conduction states.[37] The features that are observed in the near-edge region of P K-edge spectra reflect the distribution of P 3p conduction states in the rhabdophane structure while the high energy features in the spectra are likely a result of multiple scattering resonances.[37] As mentioned in the Introduction, two different PO_4 tetrahedra exist in the rhabdophane structure meaning that the P K-edge spectra from these materials contain information about the local electronic structure of both P coordination environments. In other words, the P K-edge spectrum from materials adopting the rhabdophane-type structure is a weighted average of the individual spectra arising from two coordinatively distinct P ions. Minor changes in the spectral lineshape were observed as indicated by the loss of fine structure and increase in width of the main-edge region with increasing Dy concentration (Figure 6). This change can be explained by examination of the crystal structure of rhabdophane (Figure 1a). In rhabdophane, the REO_n (n = 8 or 9) polyhedra in chains Ch1 and Ch2 are connected to each other via an alternating PO_4 tetrahedra.[12] With increasing substitution of Dy^{3+} for Gd^{3+} in $Gd_{1-x}Dy_xPO_4$, the RE-O bond lengths decreases due to the smaller ionic radii of Dy^{3+} ($r^{[VIII]}$ = 1.027 Å; $r^{[IX]}$ = 1.083 Å) ions when compared to Gd^{3+} ($r^{[VIII]}$ = 1.053 Å; $r^{[IX]}$ = 1.107 Å) ions.[34] Therefore, the local structure of the RE ion changes with increasing Dy concentration which in turn induces a slight modification in the local structure of P ions in the neighboring PO_4

tetrahedra. In the rhabdophane structure, the PO_4 tetrahedra are highly distorted due to the significant deviation of the individual O-P-O bond angles from the ideal tetrahedral angle and it is proposed here that the local symmetry around the P ion is further reduced, albeit minor, upon substitution of Dy^{3+} for Gd^{3+} in $Gd_{1-x}Dy_xPO_4$ thereby broadening the distribution of P 3p conduction states.[12] It has been shown previously that the differences in spectral lineshape observed between the P K-edge spectra of $LaPO_4$ (monazite-type) and $YbPO_4$ (xenotime-type) are a result of change in the distribution of P 3p conduction states induced by the differences in the local structure around P ions between these two structures.[37] Therefore, the differences in the spectral lineshape observed between the members of the as-synthesized $Gd_{1-x}Dy_xPO_4.H_2O$ series with increasing Dy^{3+} substitution (Figure 6) are due to an increase in the broadness of P 3p conduction states incurred by slight changes in the local environment of P ions.

P K-edge XANES spectra were also collected from $REPO_4.H_2O$ (RE = Gd, Dy) materials annealed to 600°C to investigate how the local structure around P in the rhabdophane structure was affected by the removal of water (Figures 7a and 7b). Minor differences in the P K-edge intensity were observed between the as-synthesized materials and the materials annealed at 600°C which suggests a minor change in the local structure around the P ions as a result of the removal of water (Figures 7a and 7b). This change can be explained by examination of the rhabdophane crystal structure (Figure 1). In the rhabdophane structure, the RE ions in Ch1 are coordinated to nine O ions, with eight O ions provided by the PO_4 groups and the additional O ion (colored blue in Figure 1b) being provided by water. The REO_9 polyhedra are connected to each other via PO_4 tetrahedra (Figure 1b). The removal of water from the REO_9 polyhedra may lead to a minor rearrangement of the remaining eight O ions surrounding the RE ion, and, as a consequence, the local structure of P ions in the adjoining PO_4 tetrahedra changes. In terms of

the electronic structure of the P ion, the distribution of P 3p conduction states is expected to change upon removal of water from the rhabdophane structure and, as a result, the P K-edge spectral lineshape of the material annealed at 600°C differs slightly from those of the as-synthesized material (Figure 7). It was also reported previously that the P K- and P $L_{2,3}$-edge XANES spectra from ion-implanted $REPO_4$ (RE = La, Yb) materials exhibited a loss of both intensity and fine-structure when compared to the spectrum from as-synthesized $REPO_4$ (RE = La, Yb) materials owing to a distortion of the PO_4 tetrahedra.[38] Likewise, the minor differences in lineshape observed in Figures 7a and 7b between the as-synthesized material and the material annealed at 600°C indicates a minimal change in the local symmetry of PO_4 tetrahedra upon removal of water from the rhabdophane structure. The P K-edge XANES spectra show changes in the local structure upon removal of water that were not observable by analysis of powder XRD data. When the $GdPO_4.H_2O$ and $DyPO_4.H_2O$ materials were annealed further to 1100°C, the P K-edge XANES spectra exhibited a significant change in lineshape when compared to the spectra from the as-synthesized materials and the materials annealed at 600°C. This large difference is due to the structural transformation of these materials to the monazite- ($GdPO_4$) or xenotime- ($DyPO_4$) type structure as a result of high-temperature annealing, and is in agreement with the powder XRD results presented in Section 3.1.

The local structural relationship between the rhabdophane-, monazite-, and xenotime-type structure were studied by comparing the P K-edge XANES spectra from the following materials: $GdPO_4.H_2O$ (rhabdophane-type), $GdPO_4$ (monazite-type), and $DyPO_4$ (xenotime-type) (Figure 7c). Significant variations in the P K-edge spectral lineshapes were observed and are due to a change in the distribution of P 3p conduction states in each of the three structures (Figure 7c). Focusing on the region in the energy range of 2151-2157 eV, the P K-edge spectrum from

$GdPO_4.H_2O$ does not contain fine structure (see Figure 7c) when compared to the spectra from $GdPO_4$ and $DyPO_4$. This is because the rhabdophane structure contains highly distorted PO_4 tetrahedra, resulting in non-degenerate P 3p conduction states. In the rhabdophane structure, the individual O-P-O bond angles in the PO_4 tetrahedra ranges from ~ 91.7° to 121.6° thereby indicating a significant deviation from the ideal tetrahedral angle (109.5°).[12] However, minor fine structure can be observed in the P K-edge spectra of $GdPO_4$ (Figure 7c) and indicates an increase in the number of degenerate P 3p conduction states in materials adopting the monazite structure. Although the PO_4 tetrahedra in the monazite structure is also distorted (unequal P-O bond distances and O-P-O bond angles), the magnitude of distortion in the PO_4 tetrahedra is less when compared to the rhabdophane structure due to the narrower range of O-P-O bond angles (~103.9° - 112.4°) in the monazite structure.[13] In comparison to P K-edge spectrum from $GdPO_4$ adopting the monazite-type structure, the P K-edge spectrum from $DyPO_4$ (xenotime-type) contained a more pronounced fine structure (see Figure 7c) which is due to the presence of a more symmetric PO_4 tetrahedra (similar P-O bond distances and two distinct O-P-O bond angles) that result in an increase in the number of degenerate P 3p conduction states available for 1s electrons to be excited to.[12] It should be noted that in the xenotime-type structure, the individual O-P-O bond angles in PO_4 tetrahedra are ~102.9° and ~112.9°.[13] Based on these observations, the changes in the spectral lineshape of the monazite-, rhabdophane-, and xenotime- type structures are observed to be a result of a change in the distribution of P 3p conduction states with the degree of PO_4 distortion that leads to these changes being arranged in the following order: rhabdophane (most distorted PO_4 tetrahedra) < monazite < xenotime (least distorted PO_4 tetrahedra).[37]

The effect of annealing temperature on the local structure of P in $YbPO_4.H_2O$ (xenotime-type structure) was studied by collecting P K-edge XANES spectra from $YbPO_4.H_2O$ before and after annealing (Figure 8). The P K-edge spectrum from the as-synthesized material has a lower intensity and less pronounced fine structure than the spectrum obtained from the material annealed at 1200°C (Figure 8). It is proposed here that the presence of water in the as-synthesized $YbPO_4.H_2O$ (xenotime-type structure) introduces some local disorder around P resulting in distorted PO_4 tetrahedra leading to less pronounced fine structure in the near-edge region of the P K-edge spectrum from the as-synthesized material. Similarly, it was reported that the infrared (IR) spectrum of $ErPO_4.H_2O$ (xenotime-type structure) contained additional frequency bands that were attributed to a reduction in the site-symmetry of the PO_4 tetrahedra caused by the interaction of water with the PO_4 tetrahedra.[9] The TGA data from $YbPO_4.H_2O$ showed that water was removed after heating the material to ~700°C (Figure S1b in the supporting information). Relative to the as-synthesized material, the P K-edge spectra from the material annealed at 600°C exhibited only a minor increase in intensity (Figure 8). The lack of a more pronounced fine structure in the P K-edge spectrum from the material annealed at 600°C indicates that the PO_4 tetrahedra in this material are not fully ordered (Figure 8). However, the P K-edge XANES spectrum from this material after being annealed at 1200°C has a higher intensity and greater fine-structure when compared to the spectra from the as-synthesized material and the material annealed at 600°C (Figure 8). This observation is due to a local structural transformation from distorted PO_4 tetrahedra to a more ordered PO_4 tetrahedra at higher annealing temperatures. The presence of ordered PO_4 tetrahedra leads to an increase in the number of degenerate P 3p states available for 1s electrons to be excited to, which results in the spectrum from the material annealed at 1200°C being structurally rich.

3.3. P $L_{2,3}$-edge XANES

It was shown in Section 3.2 that P K-edge XANES spectra are sensitive to temperature-induced changes in the local structure of P in materials adopting the rhabdophane- and xenotime-type structures; however, only slight changes in the lineshape of the P K-edge XANES spectra were observed for the $REPO_4.H_2O$ (RE = Gd, Dy, Yb) materials annealed at 600°C compared to the spectra from the as-synthesized materials. P $L_{2,3}$-edge spectra, which are of higher resolution when compared to P K-edge spectra, were collected from materials adopting the rhabdophane-($DyPO_4.H_2O$) type structure to determine if there is a significant change in the P $L_{2,3}$-edge spectral lineshape of $REPO_4.H_2O$ (RE = Gd, Dy, Yb) materials annealed at 600°C (Figure 9). The P $L_{2,3}$-edge spectra from $DyPO_4.H_2O$ annealed at different temperatures are shown in Figure 9 along with the spectrum from the as-synthesized material. The P $L_{2,3}$-edge spectra represent the excitation of electrons from the 2p states into unoccupied 3s and 3d states and the different features that appear in this spectra were attributed to transitions involving the overlapped P 3s and 3d conduction states.[37] The spectrum from the material annealed at 600°C is slightly broader when compared to the spectrum from the as-synthesized material confirming that the change that occurs in the local P environment upon annealing $DyPO_4.H_2O$ to 600°C is minor (Figure 9). Upon heating to 800°C, significant changes in the spectral lineshape were observed due to the structural transformation of rhabdophane to a mixture of monazite and xenotime (Figure 9). Similarly, the P $L_{2,3}$-edge spectra from the material annealed at 1100°C has a unique lineshape with greater fine-structure due to the transformation to a single phase xenotime-type structure containing a more symmetric PO_4 tetrahedra (Figure 9). It has been shown previously using partial density of states (DOS) calculations that the xenotime-type structure contains degenerate

P 3s and 3d conduction states resulting in a greater fine structure being observed in the P $L_{2,3}$-edge spectrum.[37]

3.4. RE L_3-edge XANES

The local structure of the RE (RE = Sm, Gd, Dy) ions in materials adopting the rhabdophane-type structure were studied as a function of temperature by studying the RE L_3-edge XANES spectra. The Sm L_3-edge XANES spectra from $SmPO_4.H_2O$ annealed to 600°C and 1100°C are shown in Figure 10 along with the spectra from the as-synthesized material. The white line peak in the Sm L_3-edge XANES spectra corresponds to a $2p_{3/2} \rightarrow$ 5d transition.[39,40] The Sm L_3-edge XANES spectra of the material annealed at 600°C has a slightly lower intensity compared to the spectra from the as-synthesized material that may suggest a change in the local structure of Sm brought about by the removal of water (Figure 10). Similarly, only minor changes in lineshape were observed in the Sm L_3-edge spectra of the material annealed at 1100°C despite the structural transformation from rhabdophane (as-synthesized; 600°C) to monazite at 1100°C (Figure 10). Similar results were obtained from the Gd and Dy L_3-edge XANES spectra from $(Gd,Dy)PO_4.H_2O$ (Figures S3a and S3b in the supporting information). The observation of only minor changes in the RE L_3-edge spectra with increasing annealing temperature may suggest that these spectra are not sensitive enough to detect changes in the local structure of the RE ions in these materials.

3.5. RE L_1-edge XANES

It was suggested in Section 3.4 that the RE L_3-edge XANES spectra from the $REPO_4.H_2O$ (rhabdophane-type structure) materials were not sensitive enough to detect changes in the local structure of the RE ions. The RE L_1-edge XANES spectra, on the other hand, have been

determined to be sensitive to changes in the local configuration of RE ions.[39,41,42] Sm L_1-edge spectra were collected from Sm_2O_3 and as-synthesized $SmPO_4.H_2O$ (rhabdophane-type) to determine if the Sm L_1-edge spectra can distinguish between the different coordination environments of Sm ions (Figure 11a). The Sm_2O_3 used in this study predominantly adopts the B-type monoclinic structure (C2/*c*) along with very minor amounts of C-type cubic structure.[43] The Sm L_1-edge spectra are characterized by main- and pre-edge peaks that result from dipole allowed 2s → 6p transitions and 2s → 6p-5d transitions, respectively (Figure 11a). The pre-edge peak arises as a result of the overlap of Sm 6p and 5d states which is in turn made possible due to the presence of distorted SmO_n (n = 6 - 9) polyhedra in Sm_2O_3 and $SmPO_4.H_2O$.[44,45] It should be noted that the pre-edge feature in Sm_2O_3 is more intense when compared to $SmPO_4.H_2O$ and thereby reflects the greater extent of overlap between the Sm 6p and 5d states in Sm_2O_3. Overall, the Sm L_1-edge spectrum from Sm_2O_3 (coordination number = 6 & 7) exhibited a unique lineshape in comparison to the spectrum from $SmPO_4.H_2O$ (coordination number = 8 & 9) which confirms that these spectra are sensitive to changes in the coordination environment of RE ions.

The RE (RE = Sm, Gd, Dy) L_1-edge XANES spectra were collected from $REPO_4.H_2O$ (RE = Sm, Gd, Dy) to analyze the changes in the local structure of the RE ion with increasing annealing temperature (Figure 11). Minor differences in the RE L_1-edge spectral lineshape were observed between the as-synthesized materials and the materials annealed at 600°C (Figure 11). This observation indicates that the local structure of the RE (RE = Sm, Gd, Dy) ions is only slightly affected by the removal of water from the rhabdophane-type structure. At 1100°C, the rhabdophane-type structure transforms to the monazite- ($SmPO_4$, $GdPO_4$) or xenotime- ($DyPO_4$) type structure and is accompanied by a significant change in the RE L_1-edge spectral lineshape (Figure 11). In comparison to the spectra from as-synthesized $REPO_4.H_2O$ (RE = Sm, Gd), the

RE L_1-edge spectra from $REPO_4$ (RE = Sm, Gd; monazite-type structure) exhibited greater fine structure suggesting a greater number of degenerate RE 6p conduction states in materials adopting the monazite structure compared to the rhabdophane-type structure (Figures 11a and 11b). This change in lineshape could be explained by analysis of crystal structures of rhabdophane and monazite. The rhabdophane structure contains six distinct RE ions and the corresponding REO_n (n = 8 or 9) polyhedra formed by each of these RE ions having unique RE-O bond distances.[12] In contrast, the monazite-type structure only has one distinct REO_9 polyhedra; however, the 9 RE-O bond lengths are different from each other.[13] It is proposed here that the REO_9 polyhedra in the monazite-type structure are less distorted than the REO_n (n = 8 or 9) polyhedra in the rhabdophane-type structure, resulting in a greater number of degenerate RE 6p conduction states in materials that adopt the monazite-type structure. The Dy L_1-edge spectrum from $DyPO_4$ is structurally rich as indicated by the appearance of a much more pronounced fine-structure when compared to the spectrum from $SmPO_4$ or $GdPO_4$ (cf. Figure 11). This observation can be explained by comparing the monazite and xenotime crystal structures (Figure 1). In the xenotime structure, the RE ions are coordinated to 8 O atoms and the resulting REO_8 polyhedra are symmetrical (2 distinct RE-O bond distances) when compared to the REO_9 polyhedra present in the monazite structure (Figures 1b and 1c).[13] As a result, the degeneracy of the RE 6p conduction states in the xenotime structure increases resulting in distinct fine-structure being observed in the Dy L_1-edge spectrum from $DyPO_4$ (Figure 11c). From this study, the degeneracy of RE 6p conduction states can be arranged in the following order: rhabdophane (most distorted REO_n [n = 8 or 9] polyhedra) < monazite < xenotime (least distorted REO_8 polyhedra).

Yb L_1-edge XANES spectra were collected from $YbPO_4.H_2O$ (xenotime-type) to examine how the annealing temperature influences the local structure of Yb (Figure 12). The Yb L_1-edge spectrum from the as-synthesized material has a slightly lower main-edge intensity compared to the spectrum from the materials annealed at 600°C and 1200°C (Figure 12). This observation indicates a slight distortion of the Yb coordination environment in the as-synthesized material caused by the presence of water. Upon annealing the as-synthesized material to 600°C and 1200°C, a slight increase in the main-edge intensity (~10502 eV) was observed that indicates an ordering of the local environment around the Yb^{3+} ion created by the combined effects of high temperature annealing as well as the removal of water (Figure 12).

4. Conclusion

This study has provided detailed insights into the long-range and local structures of rare-earth phosphates adopting multiple structures. Examination of powder XRD data from rhabdophane-type $DyPO_4.H_2O$ has confirmed that this material adopts the monoclinic crystal system. Temperature-induced structural variations of the rhabdophane- and xenotime- type structure were also studied using TGA, powder XRD, and XANES. Powder XRD results have shown that the anhydrous rhabdophane structure can only be stabilized over a limited temperature range (e.g., 700°C<T<800°C) whereas the xenotime-type structure was stable at all temperatures studied despite the removal of water. The local structural changes that occur upon removal of water from the rhabdophane- and xenotime- type structures were studied by collection of P K-, P $L_{2,3}$-, RE L_1-, and L_3-edge XANES spectra. The XANES studies have shown that the local symmetry of the PO_4 tetrahedra and RE-O polyhedra in $REPO_4.H_2O$ materials are modified by the removal of water. The relationship between the three rare-earth phosphates structures (rhabdophane-, monazite-, and xenotime-type structures) was also

established in this study. This study, for the first time, has shown how the local structure of $REPO_4.H_2O$ varies as a function of temperature and composition which will therefore aid in the optimization of these materials for photonics, biolabeling, catalytic, and nuclear wasteform applications.

Acknowledgements

The Natural Sciences and Engineering Research Council (NSERC) of Canada funded this project through a discovery grant awarded to APG. MRR thanks the University of Saskatchewan for financial support. MRR acknowledges the receipt of support from the CLS Graduate and Post-Doctoral Student Travel Support Program. The Canadian Foundation for Innovation (CFI) is thanked for providing funds to purchase the PANalytical Empyrean powder X-ray diffractometer that was used in this project. Drs. J. R. Hayes, P. E. R. Blanchard, and E. R. Aluri from the Department of Chemistry, University of Saskatchewan are thanked for help in the collection of the XANES spectra presented in this study. Mr. Sudheesh Kumar Veeranmaril from the Department of Chemistry, University of Saskatchewan is thanked for help in the collection of the TGA data presented in this study. Dr. Yongfeng Hu, Ms. Aimee MacLennan, and Dr. Lucia Zuin of the CLS are thanked for their support in carrying out XANES experiments at beamlines 06B1-1 and 11ID-2. Dr. Zou Finfrock is thanked for her support in carrying out XANES experiments at 20 BM (CLS@APS Sector 20, APS). The CLS is supported by NSERC, the National Research Council of Canada, the Canadian Institutes of Health Research, the Province of Saskatchewan, Western Economic Diversification Canada, and the University of Saskatchewan. Sector 20 facilities at the Advanced Photon Source, and research at these facilities, are supported by the US Department of Energy - Basic Energy Sciences, the Canadian Light Source and its funding partners, and the Advanced Photon Source. Use of the Advanced Photon Source, an Office of Science User Facility operated for the U.S. Department of Energy (DOE) Office of Science by Argonne National Laboratory, was supported by the U.S. DOE under Contract No. DE-AC02-06CH11357.

Supporting Information: Lattice constants of rhabdophane-type $Gd_{1-x}Dy_xPO_4.H_2O$; TGA plots of rhabdophane-type $DyPO_4.H_2O$ and xenotime-type $YbPO_4.H_2O$; Powder XRD patterns from $LaPO_4.H_2O$, $SmPO_4.H_2O$, and $GdPO_4.H_2O$ annealed to different temperatures; RE (RE = Sm, Gd, Dy) L_3-edge XANES spectra from $REPO_4.H_2O$ (RE = Sm, Gd, Dy).

Figure captions

Figure 1: The crystal structure of (a) rhabdophane-type $SmPO_4.0.667H_2O$ (Space group – *C*2) is shown along with the alternate arrangement of (b) Sm^{3+} and P^{5+} ions in chains Ch1 and Ch2. The crystal structures of monazite-type $CePO_4$ (Space group - $P2_1/n$), and xenotime-type YPO_4 (Space group - $I4_1/amd$) are shown in (c) and (d), respectively. The crystal structures were generated using the VESTA program.[25]

Figure 2: Rietveld refined powder XRD patterns from rhabdophane-type $DyPO_4.H_2O$ using the (a) hexagonal or (b) monoclinic structural model are shown.

Figure 3: The powder XRD patterns from the as-synthesized rhabdophane-type (a) $REPO_4.H_2O$ (RE = La, Nd, Sm, Gd, Dy) and (b) $Gd_{1-x}Dy_xPO_4.H_2O$ materials are shown.

Figure 4: The powder XRD patterns from $DyPO_4.H_2O$ annealed to (a) 600°C and 700°C and (b) 800°C and 1100°C are shown. The powder XRD pattern from as-synthesized $DyPO_4.H_2O$ material is also presented in (a) for comparison. The labels "M" and "X" in (b) have been used to identify the peaks resulting from the monazite or xenotime structure.

Figure 5: The powder XRD patterns of $YbPO_4.H_2O$ (xenotime-type structure) annealed to 600°C and 1200°C are shown along with the XRD pattern from the as-synthesized $YbPO_4.H_2O$ material.

Figure 6: The P K-edge XANES spectra from the as-synthesized $Gd_{1-x}Dy_xPO_4.H_2O$ (x = 0.0, 0.2, 0.4, 0.8, and 1.0) materials are shown.

Figure 7: The P K-edge XANES spectra from $GdPO_4.H_2O$ material annealed at 600°C and 1100°C are shown in (a) along with the spectrum from the as-synthesized material. The P K-edge

XANES spectra from $DyPO_4.H_2O$ material annealed at 600°C and 1100°C are shown in (b) along with the spectrum from the as-synthesized material. A comparison between the P K-edge XANES spectra from $GdPO_4$ (monazite-type), $GdPO_4.H_2O$ (rhabdophane-type), and $DyPO_4$ (xenotime-type) materials are shown in (c).

Figure 8: The P K-edge XANES spectra from $YbPO_4.H_2O$ annealed to 600°C and 1200°C are shown along with the spectrum from the as-synthesized material.

Figure 9: The P $L_{2,3}$-edge XANES spectra from $DyPO_4.H_2O$ annealed to 600°C, 800°C, and 1100°C are shown along with the spectrum from the as-synthesized material.

Figure 10: The Sm L_3-edge XANES spectra from $SmPO_4.H_2O$ annealed to 600°C and 1100°C are shown along with the spectrum from the as-synthesized material.

Figure 11: The Sm L_1-edge XANES spectra from $SmPO_4.H_2O$ annealed to 600°C and 1100°C are shown in (a) along with the spectrum from Sm_2O_3 and the as-synthesized material. The Gd L_1-edge XANES spectra from $GdPO_4.H_2O$ annealed to 600°C and 1100°C are shown in (b) along with the spectrum from as-synthesized material. The Dy L_1-edge XANES spectra from $DyPO_4.H_2O$ annealed to 600° and 1100°C are shown in (c) along with the spectrum from the as-synthesized material.

Figure 12: The Yb L_1-edge XANES spectra from $YbPO_4.H_2O$ annealed to 600°C and 1200°C are shown along with the spectrum from the as-synthesized material. The arrow indicates an increase in Yb L_1 main-edge intensity with increasing annealing temperature.

References

(1) Ewing, R. C.; Wang, L. Phosphates as Nuclear Waste Forms. *Rev. Mineral. Geochemistry* **2002**, *48*, 673–699.

(2) Oelkers, E. H.; Montel, J.-M. Phosphates and Nuclear Waste Storage. *Elements* **2008**, *4*, 113–116.

(3) Li, H.; Zhu, G.; Ren, H.; Li, Y.; Hewitt, I. J.; Qiu, S. The Synthesis of Multiwalled Rare-Earth Phosphate Nanomaterials using Organophosphates with Upconversion Properties. *Eur. J. Inorg. Chem.* **2008**, *2008*, 2033–2037.

(4) Wang, L.; He, D.; Feng, S.; Yu, C.; Hu, L.; Qiu, J.; Chen, D. Phosphate Ytterbium-doped Single-mode All-Solid Photonic Crystal Fiber with Output Power of 13.8 W. *Sci. Rep.* **2015**, *5*, 8490.

(5) Kitamura, N.; Amezawa, K.; Tomii, Y.; Yamamoto, N. Protonic Conduction in Rare-Earth Orthophosphates with the Monazite Structure. *Solid State Ionics* **2003**, *162–163*, 161–165.

(6) Anfimova, T.; Li, Q.; Jensen, J. O.; Bjerrum, N. J. Thermal Stability and Proton Conductivity of Rare-Earth Orthophosphate Hydrates. *Int. J. Electrochem. Sci.* **2014**, *9*, 2285–2300.

(7) Onoda, H.; Nariai, H.; Moriwaki, A.; Maki, H.; Motooka, I. Formation and Catalytic Characterization of Various Rare Earth Phosphates. *J. Mater. Chem.* **2002**, *12*, 1754–1760.

(8) Meiser, F.; Cortez, C.; Caruso, F. Biofunctionalization of Fluorescent Rare-Earth-Doped

Lanthanum Phosphate Colloidal Nanoparticles. *Angew. Chemie Int. Ed.* **2004**, *43*, 5954–5957.

(9) Kijkowska, R. Thermal Decomposition of Lanthanide Orthophosphates Synthesized Through Crystallisation from Phosphoric Acid Solution. *Thermochim. Acta* **2003**, *404*, 81–88.

(10) Mooney, R. C. L. Crystal Structures of a Series of Rare-Earth Phosphates. *J. Chem. Phys.* **1948**, *16*, 1003.

(11) Mooney, R. C. L. X-ray Diffraction Study of Cerous Phosphate and Related Crystals. I. Hexagonal Modification. *Acta Crystallogr.* **1950**, *3*, 337–340.

(12) Mesbah, A.; Clavier, N.; Elkaim, E.; Gausse, C.; Kacem, I. Ben; Szenknect, S.; Dacheux, N. Monoclinic Form of the Rhabdophane Compounds: $REEPO_4.0.667H_2O$. *Cryst. Growth Des.* **2014**, *14*, 5090–5098.

(13) Ni, Y.; Hughes, J. M.; Mariano, A. N. Crystal Chemistry of the Monazite and Xenotime Structures. *Am. Mineral.* **1995**, *80*, 21–26.

(14) Ewing, R. C. Nuclear Waste Forms for Actinides. *Proc. Natl. Acad. Sci.* **1999**, *96*, 3432–3439.

(15) Schlenz, H.; Heuser, J.; Neumann, A.; Schmitz, S.; Bosbach, D. Monazite as a Suitable Actinide Waste Form. *Zeitschrift für Krist.* **2013**, *228*, 113–123.

(16) Du Fou de Kerdaniel, E.; Clavier, N.; Dacheux, N.; Terra, O.; Podor, R. Actinide Solubility-Controlling Phases during the Dissolution of Phosphate Ceramics. *J. Nucl. Mater.* **2007**, *362*, 451–458.

(17) Boatner, L. A. Synthesis, Structure, and Properties of Monazite, Pretulite, and Xenotime. *Rev. Mineral. Geochemistry* **2002**, *48*, 87–121.

(18) Kijkowska, R. Preparation of Lanthanide Orthophosphates. *J. Mater. Sci.* **2003**, *8*, 229–233.

(19) Mayence, A.; Navarro, J. R. G.; Ma, Y.; Terasaki, O.; Bergstro, L. Phase Identification and Structure Solution by Three-Dimensional Electron Diffraction Tomography: Gd-Phosphate Nanorods. *Inorg. Chem.* **2014**, *53*, 5067–5072.

(20) Ferhi, M.; Horchani-Naifer, K.; Férid, M. Hydrothermal Synthesis and Photoluminescence of the Monophosphate $LaPO_4$:Eu(5%). *J. Lumin.* **2008**, *128*, 1777–1782.

(21) Lu, S.; Zhang, J.; Zhang, J.; Zhao, H.; Luo, Y.; Ren, X. Remarkably Enhanced Photoluminescence of Hexagonal $GdPO_4.nH_2O$:Eu with Decreasing Size. *Nanotechnology* **2010**, *21*, 365709.

(22) Di, W.; Li, J.; Shirahata, N.; Sakka, Y.; Willinger, M.-G.; Pinna, N. Photoluminescence, Cytotoxicity, and In Vitro Imaging of Hexagonal Terbium Phosphate Nanoparticles Doped with Europium. *Nanoscale* **2011**, *3*, 1263–1269.

(23) Wang, X.; Gao, M. A Facile Route for Preparing Rhabdophane Rare Earth Phosphate Nanorods. *J. Mater. Chem.* **2006**, *16*, 1360–1365.

(24) Valérie, B.; Mélanie, M.; Thierry, G.; Jean-Pierre, B.; Jean-Yves C.-C; Thierry, L. M. Colloidal Synthesis of Luminescent Rhabdophane $LaPO_4:Ln^{3+}.xH_2O$ (Ln = Ce, Tb, Eu; x ~ 0.7) Nanocrystals. *Chem. Mater.* **2004**, *16*, 3767–3773.

(25) Momma, K.; Izumi, F. VESTA: A Three-Dimensional Visualization System for Electronic

and Structural Analysis. *J. Appl. Crystallogr.* **2008**, *41*, 653–658.

(26) Clavier, N.; Podor, R.; Dacheux, N. Crystal Chemistry of the Monazite Structure. *J. Eur. Ceram. Soc.* **2011**, *31*, 941–976.

(27) De Groot, F. High-Resolution X-ray Emission and X-ray Absorption Spectroscopy. *Chem. Rev.* **2001**, *101*, 1779–1808.

(28) Degen, T.; Sadki, M.; Bron, E.; König, U.; Nénert, G. The HighScore Suite. *Powder Diffr.* **2014**, *29* (Supplement S2), S13–S18.

(29) Hu, Y. F.; Coulthard, I.; Chevrier, D.; Wright, G.; Igarashi, R.; Sitnikov, A.; Yates, B. W.; Hallin, E. L.; Sham, T. K.; Reininger, R. Preliminary Commissioning and Performance of the Soft X-ray Micro-Characterization Beamline at the Canadian Light Source. *AIP Conference Proceedings,* **2010**, 1234, 343–346.

(30) Thompson, A.; Attwood, D.; Gullikson, E. M.; Howells, M.; Kim, K.--J.; Kirz, J.; Kortright, J.; Lindau, I.; Yanwei, L.; Pianetta, P.; Robinson, A.; Scofield, J.; Underwood, J.; Williams, G.; Winick, H. *X-ray data booklet*; Lawrence Berkeley National Laboratory; 2001; Vol. 8.

(31) Ravel, B.; Newville, M. ATHENA, ARTEMIS, HEPHAESTUS: Data Analysis for X-ray Absorption Spectroscopy using IFEFFIT. *J. Synchrotron Radiat.* **2005**, *12*, 537–541.

(32) Hu, Y. F.; Zuin, L.; Reininger, R.; Sham, T. K. VLS-PGM beamline at the Canadian Light Source. In *AIP Conference Proceedings,* **2007**, 879, 535–538.

(33) Heald, S. M.; Brewe, D. L.; Stern, E. A.; Kim, K. H.; Brown, F. C.; Jiang, D. T.; Crozier, E. D.; Gordon, R. A. XAFS and Micro-XAFS at the PNC-CAT Beamlines. *J. Synchrotron*

Radiat. **1999**, *6*, 347–349.

(34) Shannon, R. D. Revised Effective Ionic Radii and Systematic Studies of Interatomic Distances in Halides and Chalcogenides. *Acta Crystallogr. Sect. A* **1976**, *32*, 751–767.

(35) Lucas, S.; Champion, E.; Bernache-Assollant, D.; Leroy, G. Rare Earth Phosphate Powders $REPO_4.nH_2O$ (RE = La, Ce or Y) II. Thermal Behavior. *J. Solid State Chem.* **2004**, *177*, 1312–1320.

(36) Lucas, S.; Champion, E.; Bregiroux, D.; Bernache-Assollant, D.; Audubert, F. Rare Earth Phosphate Powders $REPO_4.nH_2O$ (RE = La, Ce or Y) - Part I. Synthesis and Characterization. *J. Solid State Chem.* **2004**, *177*, 1302–1311.

(37) Rafiuddin, M. R.; Mueller, E.; Grosvenor, A. P. X-ray Spectroscopic Study of the Electronic Structure of Monazite- and Xenotime- Type Rare-Earth Phosphates. *J. Phys. Chem. C* **2014**, *118*, 18000–18009.

(38) Rafiuddin, M. R.; Grosvenor, A. P. Probing the Effect of Radiation Damage on the Structure of Rare-Earth Phosphates. *J. Alloys Compd.* **2015**, *653*, 279–289.

(39) Asakura, H.; Shishido, T.; Fuchi, S.; Teramura, K.; Tanaka, T. Local Structure of Pr, Nd, and Sm Complex Oxides and their X-ray Absorption Near-edge Structure Spectra. *J. Phys. Chem. C* **2014**, *118*, 20881–20888.

(40) Ishii, M.; Crowe, I. F.; Halsall, M. P.; Hamilton, B.; Hu, Y.; Sham, T.-K.; Harako, S.; Zhao, X.-W.; Komuro, S. Atomic Scale Distortion of Optically Activated Sm Dopants Identified with Site-Selective X-ray Absorption Spectroscopy. *J. Appl. Phys.* **2013**, *114*, 133505.

(41) Asakura, H.; Shishido, T.; Teramura, K.; Tanaka, T. Local Structure and La L_1- and L_3-Edge XANES Spectra of Lanthanum Complex Oxides. *Inorg. Chem.* **2014**, *53*, 6048–6053.

(42) Asakura, H.; Shishido, T.; Teramura, K.; Tanaka, T. Local Structure and L_1- and L_3-edge X-ray Absorption Near-Edge Structure of Late Lanthanide Elements (Ho, Er, Yb) in their Complex Oxides. *J. Phys. Chem. C* **2015**, *119*, 8070–8077.

(43) Kennedy, B. J.; Avdeev, M. The Structure of B-type Sm_2O_3. A Powder Neutron Diffraction Study using Enriched ^{154}Sm. *Solid State Sci.* **2011**, *13*, 1701–1703.

(44) Yamazoe, S.; Hitomi, Y.; Shishido, T.; Tanaka, T. XAFS Study of Tungsten L_1- and L_3-Edges: Structural Analysis of WO_3 Species Loaded on TiO_2 as a Catalyst for Photo-oxidation of NH_3. *J. Phys. Chem. C* **2008**, 112, 6869–6879.

(45) Yamamoto, T. Assignment of Pre-Edge peaks in K-edge Absorption Spectra of 3d Transition Metal Compounds: Electric Dipole or Quadrupole?. *X-Ray Spectrom.* **2008**, *37*, 572–584.

Tables

Table 1: Lattice constants and Rietveld refinement results for $DyPO_4.H_2O$

Crystal system	Lattice constants	B_{OVL}	Agreement indices
Hexagonal[a]	a = 6.8476 (3)	2.81 (12)	R_{wp}[b] = 17.60
	c = 6.3084 (3)		R_p[c] = 12.91
			R_{exp}[d] = 3.48
			χ^2[e] = 25.65
Monoclinic	a = 27.874 (1)	3.77 (4)	R_{wp} = 6.65
	b = 6.8485 (5)		R_p = 5.37
	c = 11.8596 (9)		R_{exp} = 3.60
	β = 115.141 (5)		χ^2 = 3.42

[a]The a and b lattice constants are identical in the hexagonal unit cell

[b]Weighted profile R-factor, $R_{wp} = \left[\frac{\sum(w_i(y_{i(obs)}-y_{i(calc)})^2}{\sum w_i y_{i(obs)}{}^2}\right]^{1/2}$

[c]Profile R-factor, $R_P = \frac{\sum |y_{i(obs)}- y_{i(calc)}|}{\sum y_{i(obs)}}$

[d]Expected R-factor, $R_{exp} = \left[\frac{N-P}{\sum w_i y_{i(obs)}{}^2}\right]^{1/2}$

where, N = number of observations; P = number of estimated least square parameters

[e]Goodness of fit, $\chi^2 = \left[\frac{R_{wp}}{R_{exp}}\right]^2$

Table 2: Lattice constants from as-synthesized rhabdophane-type $REPO_4.H_2O$ materials

Compounds	a (Å)	b (Å)	c (Å)	β (degrees)
$LaPO_4.H_2O$	28.740 (5)	7.136 (1)	12.267 (2)	115.34 (2)
$NdPO_4.H_2O$	28.309 (6)	7.028 (1)	12.100 (2)	115.40 (2)
$SmPO_4.H_2O$	28.162 (3)	6.956 (1)	12.037 (2)	115.36 (1)
$GdPO_4.H_2O$	27.997 (3)	6.907 (1)	11.971 (2)	115.25 (1)
$DyPO_4.H_2O$	27.874 (1)	6.8485 (5)	11.8595 (9)	115.141 (5)

Table 3: Lattice constants from as-synthesized and annealed xenotime-type $YbPO_4.H_2O$

Sample	a (Å)	c (Å)
As-synthesized	6.8405 (4)	5.9927 (4)
Annealed at 600°C	6.8147 (8)	5.9785 (4)
Annealed at 1200°C	6.8162 (2)	5.9706 (2)

Figure 1

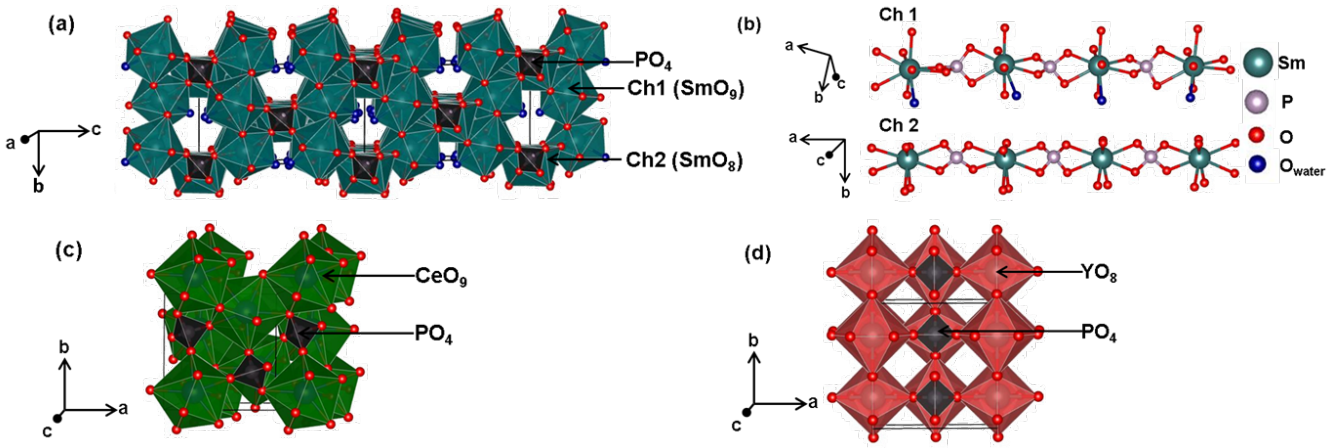
(a)
PO4
Ch1 (SmO9)
Ch2 (SmO8)
a
c
b
(b)
Ch 1
Ch 2
Sm
P
O
Owater
(c)
CeO9
PO4
(d)
YO8
PO4

Figure 2

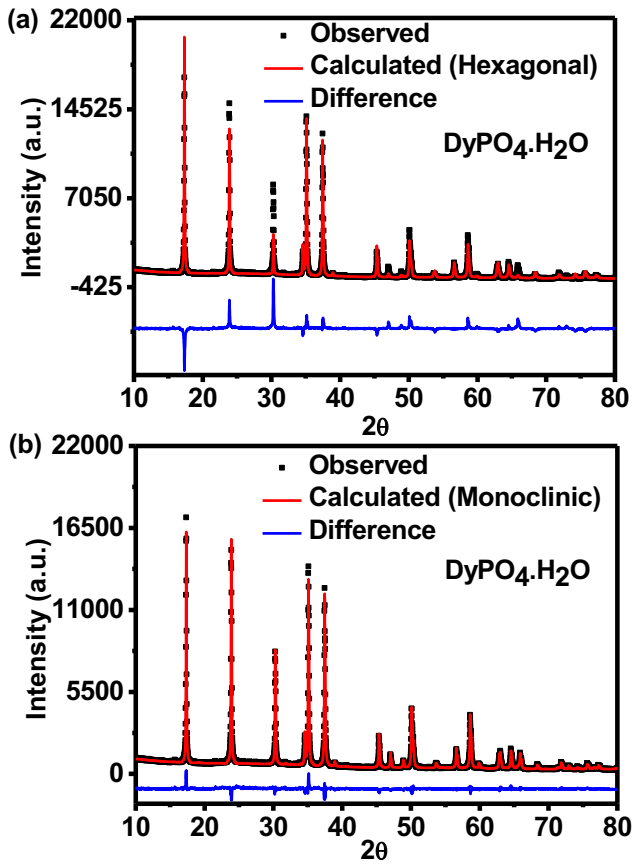
(a)
22000
14525
7050
-425
Intensity (a.u.)
Observed
Calculated (Hexagonal)
Difference
DyPO4.H2O
10
20
30
40
50
60
70
80
2θ
(b)
22000
16500
11000
5500
0
Intensity (a.u.)
Observed
Calculated (Monoclinic)
Difference
DyPO4.H2O
10
20
30
40
50
60
70
80
2θ

Figure 3

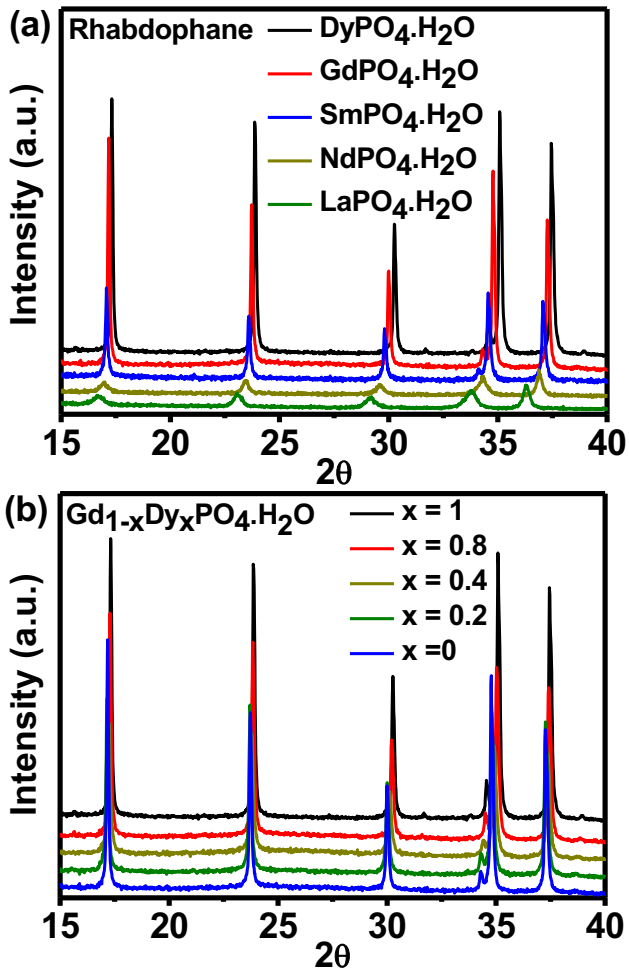
(a)
Rhabdophane
DyPO4.H2O
GdPO4.H2O
SmPO4.H2O
NdPO4.H2O
LaPO4.H2O
Intensity (a.u.)
15
20
25
30
35
40
2θ
(b)
Gd1-xDyxPO4.H2O
x = 1
x = 0.8
x = 0.4
x = 0.2
x =0
Intensity (a.u.)
15
20
25
30
35
40
2θ

Figure 4

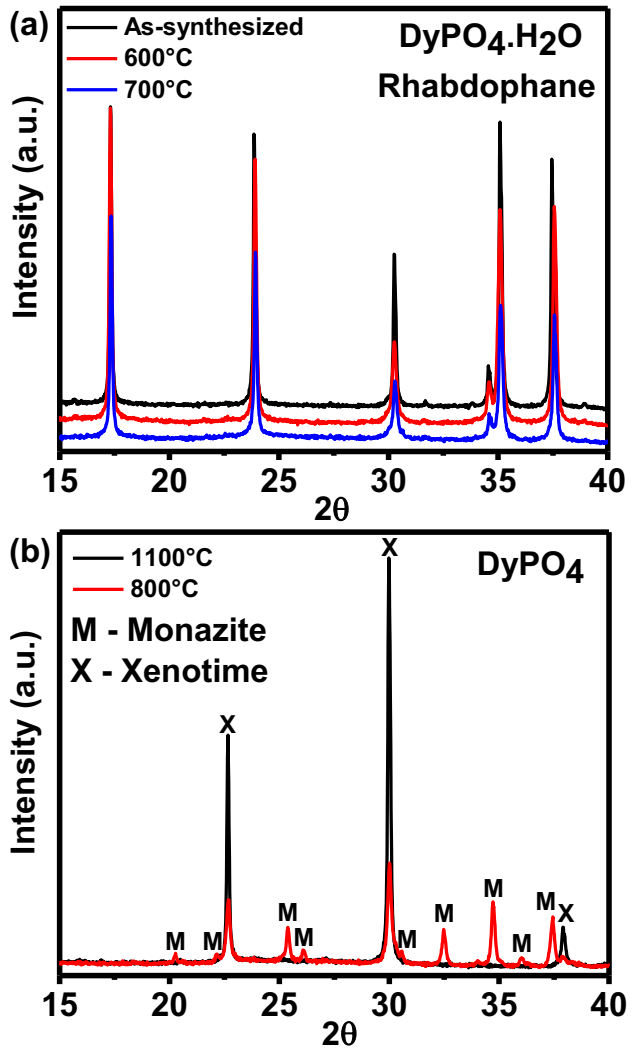
(a)
As-synthesized
600°C
700°C
DyPO4.H2O
Rhabdophane
Intensity (a.u.)
15
20
25
30
35
40
2θ
(b)
1100°C
800°C
DyPO4
M - Monazite
X - Xenotime
Intensity (a.u.)
X
M
M
M
M
M
M
M
M
X
15
20
25
30
35
40
2θ

Figure 5

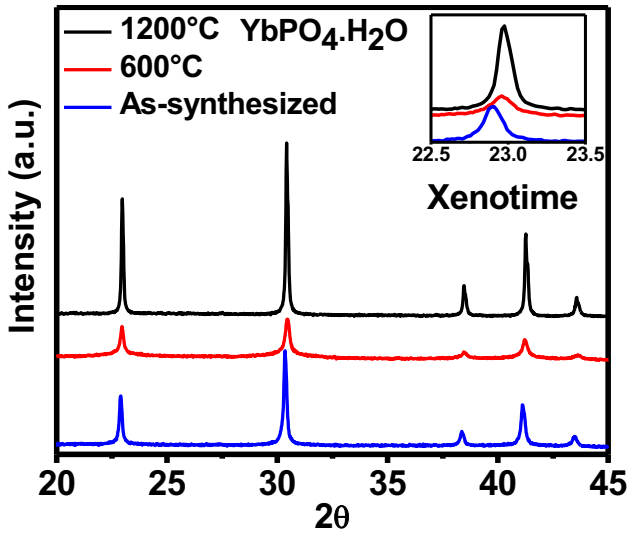
1200°C YbPO4.H2O
600°C
As-synthesized
Intensity (a.u.)
20
25
30
35
40
45
2θ
22.5
23.0
23.5
Xenotime

Figure 6

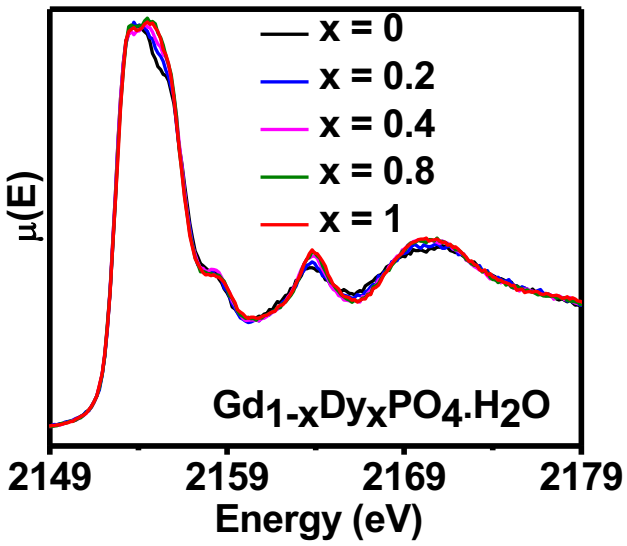
x = 0
x = 0.2
x = 0.4
x = 0.8
x = 1
μ(E)
Gd1-xDyxPO4.H2O
2149
2159
2169
2179
Energy (eV)

Figure 7

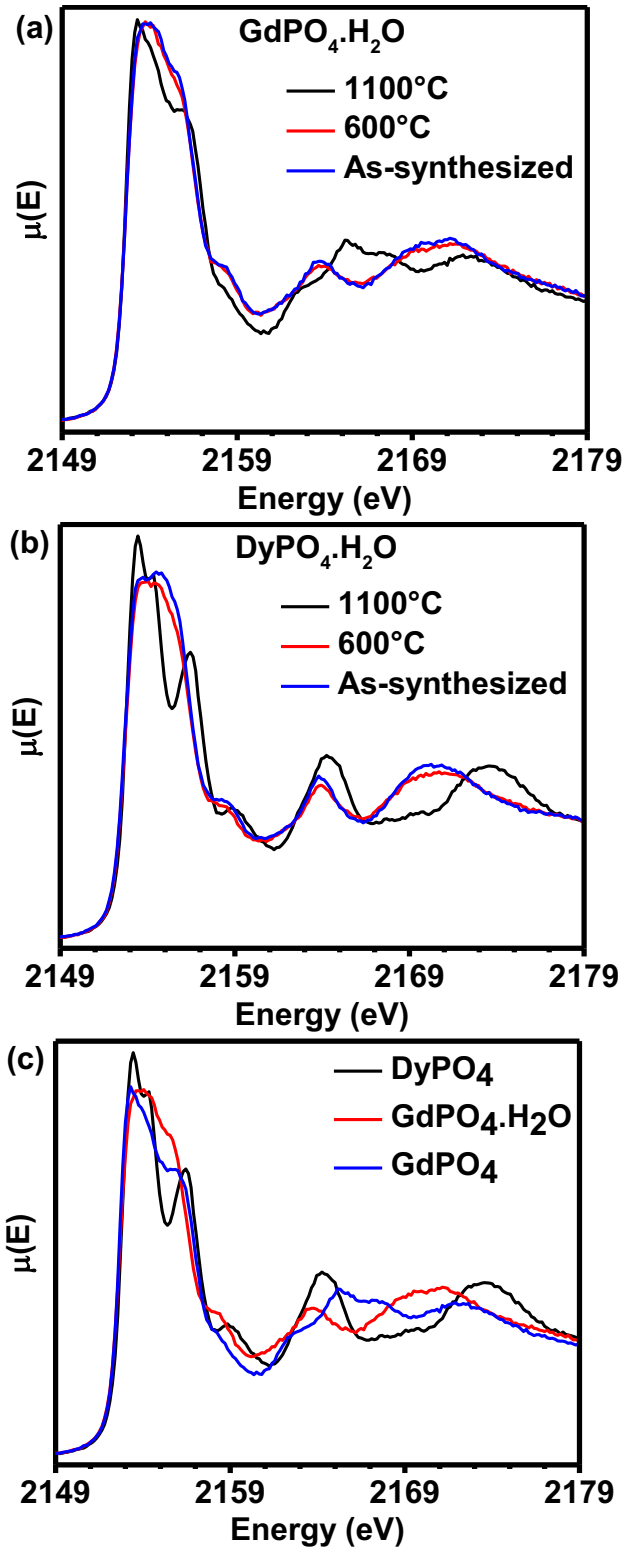
(a)
GdPO4.H2O
1100°C
600°C
As-synthesized
μ(E)
2149
2159
2169
2179
Energy (eV)
(b)
DyPO4.H2O
1100°C
600°C
As-synthesized
μ(E)
2149
2159
2169
2179
Energy (eV)
(c)
DyPO4
GdPO4.H2O
GdPO4
μ(E)
2149
2159
2169
2179
Energy (eV)

Figure 8

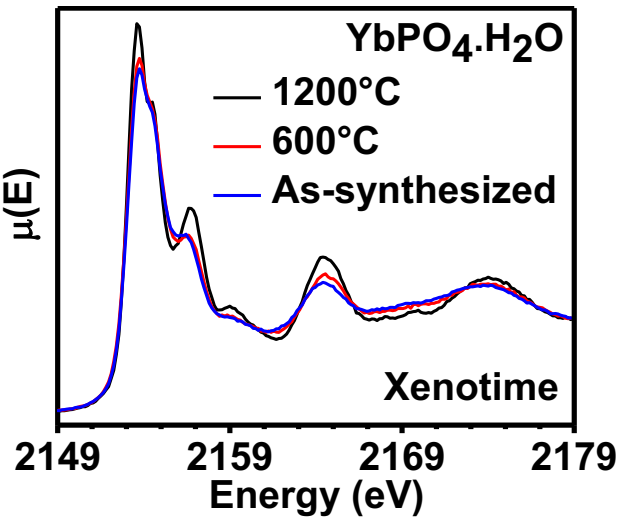
YbPO4.H2O
1200°C
600°C
As-synthesized
Xenotime
μ(E)
2149
2159
2169
2179
Energy (eV)

Figure 9

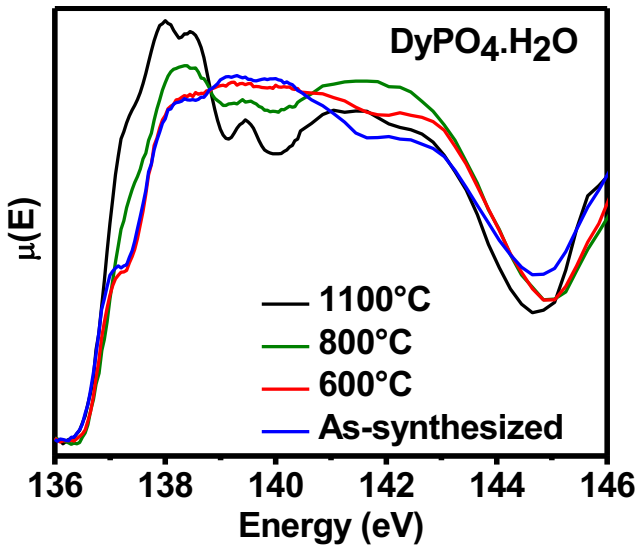
DyPO4.H2O
μ(E)
1100°C
800°C
600°C
As-synthesized
136
138
140
142
144
146
Energy (eV)

Figure 10

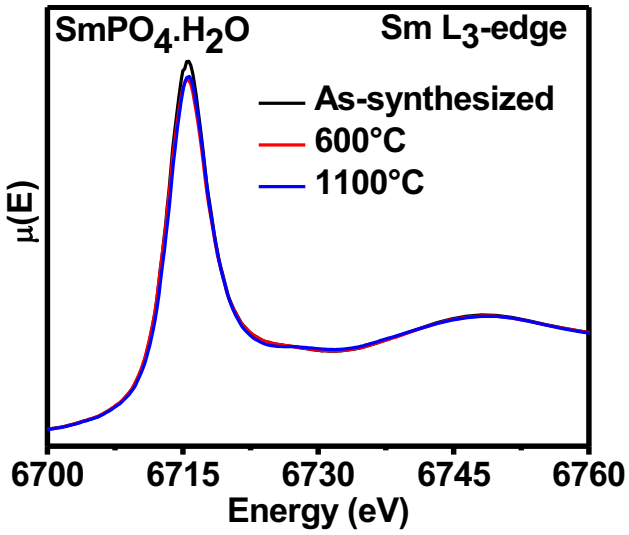
SmPO4.H2O
Sm L3-edge
As-synthesized
600°C
1100°C
μ(E)
6700
6715
6730
6745
6760
Energy (eV)

Figure 11

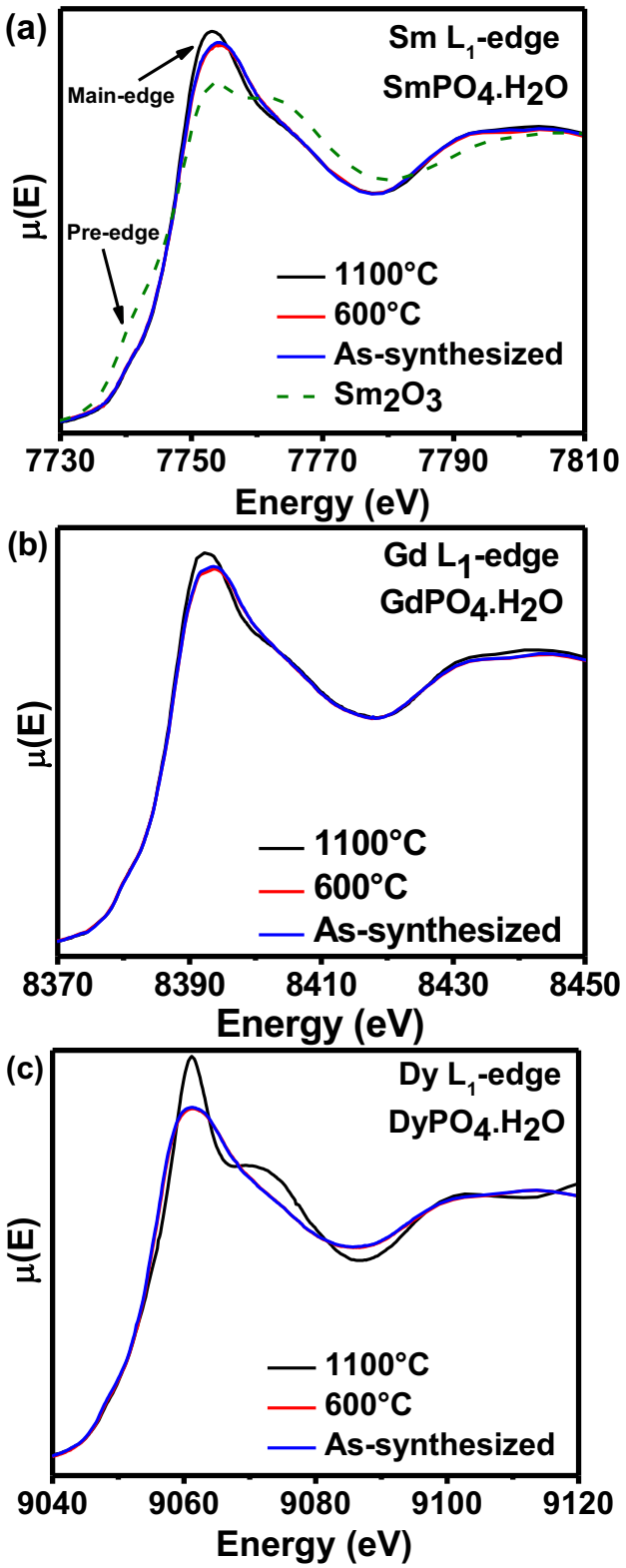
(a)
Sm L1-edge
SmPO4.H2O
Main-edge
Pre-edge
μ(E)
1100°C
600°C
As-synthesized
Sm2O3
7730
7750
7770
7790
7810
Energy (eV)
(b)
Gd L1-edge
GdPO4.H2O
μ(E)
1100°C
600°C
As-synthesized
8370
8390
8410
8430
8450
Energy (eV)
(c)
Dy L1-edge
DyPO4.H2O
μ(E)
1100°C
600°C
As-synthesized
9040
9060
9080
9100
9120
Energy (eV)

Figure 12

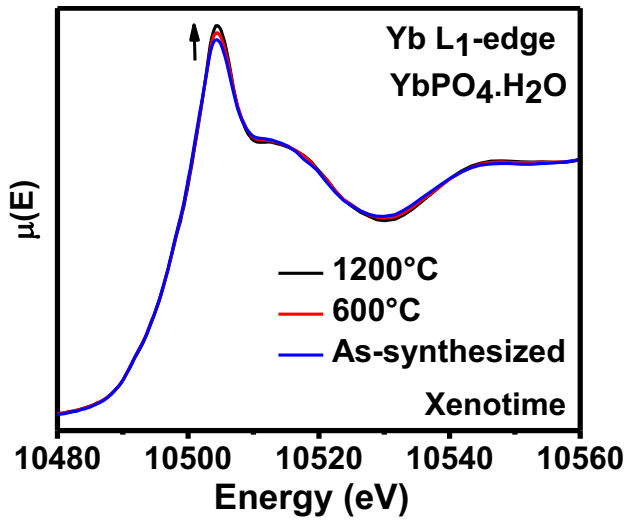
Yb L1-edge
YbPO4.H2O
μ(E)
1200°C
600°C
As-synthesized
Xenotime
10480
10500
10520
10540
10560
Energy (eV)

For Table of Contents Only:

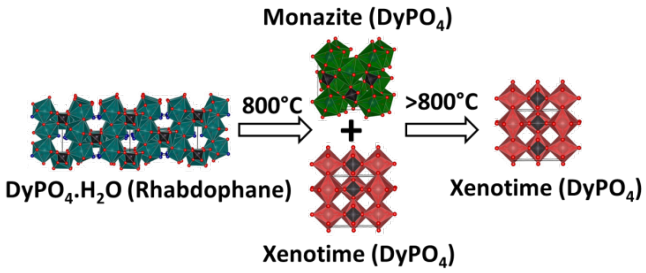

Rare-earth phosphates ($REPO_4$ & $REPO_4.nH_2O$) have wide-ranging applications (e.g., as nuclear wasteforms and in photonics) that are composition and structure dependent. In this study, hydrous and anhydrous rare-earth phosphates were synthesized and their long-range and local structures were studied using powder X-ray diffraction (XRD) and X-ray absorption near-edge spectroscopy (XANES). Rhabdophane-type ($REPO_4.nH_2O$) materials are metastable and transform to either monazite- or xenotime-type structures at higher annealing temperatures depending on the size of rare-earth ion.